Optical Engineering

SPIEDigitalLibrary.org/oe

Lightweight hollow rooftop mirrors for stabilized interferometry

Robert J. Hill
Trevor L. Courtney
Samuel D. Park
David M. Jonas

SPIE

Lightweight hollow rooftop mirrors for stabilized interferometry

Robert J. Hill
University of Colorado
Department of Physics
Boulder, Colorado 80309-0390

Trevor L. Courtney
Samuel D. Park
David M. Jonas
University of Colorado
Department of Chemistry and Biochemistry
Boulder, Colorado 80309-0215
E-mail: david.jonas@colorado.edu.

Abstract. Hollow rooftop mirrors, also known as dihedral retroreflectors, can simultaneously preserve polarization, minimize chromatic dispersion, and allow beams to be stacked inside an interferometer. Two hollow rooftop mirrors were fabricated and characterized using a Fizeau interferometer and an inexpensive home-built jig instead of a master cube. The mass was 3.3 g for a clear aperture surface area of 110 mm^2 with maximum retroreflected beam deviation of 12 arc s. With a hollow rooftop mirror mounted on a piezoelectric transducer in one arm of a Mach-Zehnder interferometer, a displacement stability of ± 0.8 nm rms was achieved using active feedback. The rooftop mirrors' suitability for Fourier transform spectroscopy was demonstrated. [DOI: 10.1117/1.OE.52.10.105103]

Subject terms: retroreflector; hollow rooftop mirror; hollow roof mirror; actively stabilized interferometer; dihedral retroreflector; Porro mirror; hollow Porro prism.

Paper 130962 received Jun. 27, 2013; revised manuscript received Aug. 30, 2013; accepted for publication Sep. 13, 2013; published online Oct. 4, 2013.

1 Introduction

Retroreflectors have found many precision metrology uses, from measurements of distances[1] and machining,[2] to stabilized[3] and scanning interferometers.[4] The main advantage of using a retroreflector over a mirror is that it returns the light to its source without great sensitivity to alignment.[5] While there are many retroreflector designs, hollow retroreflectors serve an important role in Fourier transform spectroscopy,[6] laser stabilization,[7] and interference-based ultrafast techniques.[3,4] Hollow retroreflectors are preferred over other designs because they have lower masses than solid retroreflectors. They also minimize the chromatic dispersion that lengthens ultrafast pulses. For ultrafast spectroscopy, stabilization is often accomplished by 90 deg reflection from a single displacement-stabilized mirror, but this leads to phase shifts that are readily detectable with Fourier transform spectral interferometry.[8] These phase shifts can be eliminated by mounting retroreflectors on piezoelectric transducers.[3]

Hollow rooftop mirrors (HRMs) allow beams to be stacked without inversion of the stack and can preserve polarization (unlike trihedral retroreflectors). For a 90 deg angle between plane mirror surfaces, HRMs retroreflect light incident in planes perpendicular to the mirror joint axis (dihedral retroreflection). The drawbacks to HRMs are that dihedral retroreflection is sensitive to the inclination angle of the incident beam to the mirror joint axis,[6] that the polarization and stacking advantages are sensitive to rotation of the rooftop mirror in the plane of the aperture, and that preservation of *s* or *p* polarization is sensitive to the inclination angle.

A reflector's mass limits the achievable bandwidth governing displacement-stability in interferometers,[9] providing motivation to reduce retroreflector mass in order to achieve greater displacement-stability. The primary difficulty in constructing hollow rooftop[10] and trihedral[11] retroreflectors can be traced to the mechanical design joining the mirrors. This challenge becomes amplified when scaling down to smaller and lighter retroreflectors that can have reduced contact area between mirrors, in contrast to difficulties encountered when scaling up the size of prisms.[12] References that discuss solid prism fabrication[13] mention solid retroreflectors as master cubes for hollow retroreflectors, but a detailed description of hollow trihedral (corner cube) retroreflector fabrication[11,14] is rare; in particular, critical bonding materials are usually omitted as proprietary.[10,15–17] One route involves assembly of coated mirrors in a permanent support structure followed by measurement and adjustment while bonding and curing;[16,17] the other involves assembly and direct bonding of uncoated mirrors on a master prism, followed by coating.[10,11] The method presented here bonds coated mirrors directly while measuring and adjusting the dihedral angle, allowing fabrication of HRMs that are lighter and have a greater surface area to mass ratio than those commercially available.[17]

2 Experimental

Two HRMs were each constructed[18] from a rectangular "enhanced silver broadband visible and infrared metal and dielectric mirror" with a $\lambda/10$ front surface at 632 nm (JML MPS 14407/309—suffix 309 indicates coating with metallic silver and a protective dielectric overcoat designed for reflectance over 98% across the 500 to 1100 nm wavelength range and for cleaning with water, alcohol, and acetone;[19] this coating has different specifications from the reflective coating with suffix 309 currently on the JML web site[20]). Mirror dimensions were 17.8 mm × 13.8 mm, with a 3.2 mm Pyrex® substrate thickness. The mirror was cut into two pieces with a low-speed diamond wheel saw (South Bay Technology® Model 650, typically used for cutting semiconductor wafers), using a 3 in. diameter, 0.006 in. thick blade. Letting a represent the thickness of the glass substrate, the total length (17.8 mm here) is cut into two pieces with lengths L and $L + a$, making $L =$ 7.3 mm. This gives each HRM a maximum total projected area of 10.3 mm × 13.8 mm.

A jig was constructed by bolting two kinematic mirror mounts (New Focus, 9809 Classic Corner Mirror Mounts) to the plane of a free standing aluminum block wall. The mirror mounts formed a 90 deg V angle with each mirror at 45 deg angle with respect to the base of the block wall. The two mirror halves were placed in the V groove with their mirrored surfaces facing up, as shown in Fig. 1.

A Fizeau interferometer[21,22] (Zygo, GPI-XP, using the Metropro software app for characterizing the surface height of flats—the Metropro corner cube app was not available) characterizes the two-dimensional phase profile by sending out a 632.8-nm wavelength helium neon laser plane wave to reflect off the HRMs and interfere with a reference plane wave. In this single pass test,[23] the reflected rays follow optical paths from the reference plane down to the first mirror, across to the second mirror, and back up to the reference plane. With respect to a reference, bright fringes represent phase differences of $2n\pi$ (integers n), while alternating dark fringes represent phase differences of $(2n+1)\pi$. The wavefront difference (in waves) between two rays measured with a Fizeau interferometer equals the quotient of the optical pathlength difference between those two rays divided by the measuring wavelength (for a mirror, the optical pathlength difference is exactly twice the surface height difference). Asymmetrical wavefront errors introduced by the interferometer will appear twice as severe as they really are in a single pass test, and all measured asymmetries across the mirror joint axis in the returned wavefront arise from the interferometer.[23]

To achieve the final result, mirror angles were aligned in the jig three times while monitoring the interference fringes. The first alignment sets the jig up correctly with the mirrors simply resting on it; this alignment step is necessary because the mirror of length $L+a$ makes contact with both mirror mounts of the jig (see Fig. 1). A single fringe across the entire surface rendered the two mirrors nearly indistinguishable from a flat mirror and was indicative of an ideal 90 deg angle whose continuity was broken by a thin line where the two halves were joined. To set the approximate bonding angle and position, the mirror of length $L+a$ was then affixed to one mirror mount with a layer of molten thermopolymer (Crystalbond™ 509 washable adhesive, soluble in acetone, flowpoint 121°C) less than ~0.25 mm thick as judged by eye. The shorter mirror was then slid into position

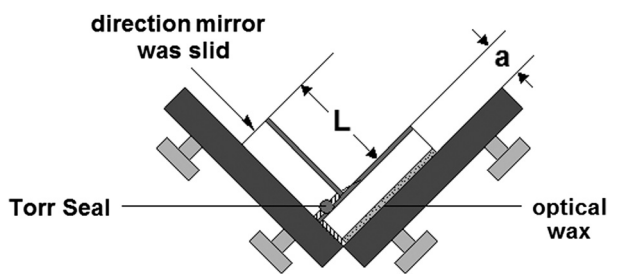

Fig. 1 Mirror positioning on the jig. The coated mirror surfaces are uppermost (medium gray); the mirror sides cut with the diamond saw are marked with diagonal hatching. The longer mirror was firmly affixed to the optics mount (on the right) by pressing it into a thin layer of molten thermopolymer adhesive (dotted light gray). To prevent smearing Torr Seal® on the longer mirror, the shorter mirror was slid in the direction of the arrow along the optic mount into its bonding position to form a 90 deg contact-angle with the longer mirror.

using the mirror mount as a guide ramp until the side cut with the diamond saw rested on the reflective surface of the longer mirror (Fig. 1). In preparation for bonding, a second alignment restored a single fringe across both mirrors. Then, a thin (width ~1 mm as judged by eye on the 3.2 mm thick substrate) bead of adhesive (Torr Seal®, Varian) was applied to the cut side of the shorter mirror with a toothpick and it was slid back into position, bonding the two mirrors. The third alignment took place immediately after this application of adhesive to the joint between mirrors.

While the adhesive cured during the first two hours, small and incremental adjustments were made to the dihedral angle. As the adhesive dried completely, smaller drifts, typically much less than $\lambda/20$ occurred over the following ~24 h. Heating the underside of the optical mount allowed removal of the HRM from the thermopolymer adhesive without softening the Torr Seal® at the HRM joint.

Using Torr Seal® as the adhesive was crucial. A number of bonding agents were attempted without success, including cyanoacrylate[24] (Duro Super Glue), UV curable epoxy adhesive (Epo-Tek OG116), two component thermally cured epoxy (Epo-Tek 353ND), two part epoxy (Hardman Double/Bubble Extra Fast Setting Epoxy), and white glue (Elmer's Glue-All). The common problem was that large changes in the angle between mirrors occurred while curing. Two adhesives [Stycast 2850 with catalyst 9 (Emerson and Cuming) was found to have lower thermal expansion than EPON Resin 828 with curing agent Versamid 140] and a tongue and groove assembly for minimizing such changes have been discussed,[11] as has hydroxide bonding of uncoated substrates.[14] Exploration of specialized bonding cements and additives[11,14,24,25] was inhibited by cost. Torr Seal®, on the other hand, has long been used for bonding Brewster windows[26] and end mirrors in stabilized laser cavities, suggesting that angles can be set and that it forms a mechanically stable bond compatible with an actively stabilized interferometer element. The high Young's modulus of Torr Seal® has proven useful in mounting tuning fork tips for atomic force microscopy.[27] Torr Seal® is a high vacuum adhesive with a high specified[28] shear strength of 13.8 MPa (2000 psi), a useful temperature range of −45 to 120°C, a low coefficient of thermal expansion of $30.3\times10^{\times6}/°C$, and a high Young's modulus [estimates from the specified Shore D hardness of 75 to 80 range from ~400 MPa using Fig. 11 of Ref. 29 to ~9 GPa (Ref. 27)]; compared to representative structural adhesives,[25] all of these suggest Torr Seal® can be useful for mounting optics.

To prevent bending of the HRM, side supports (also called end plates[24] or end braces) were added. For low mass, these reinforcements were constructed of glass microscope cover slips (VWR Micro Cover Glasses, #48366-205, 18 mm × 18 mm × 0.18 mm) cut into a shape resembling a Superman© shield (see Fig. 2) and attached with Torr Seal®. After pressing the support into place, the HRM was positioned so that the support was on top of the HRM as the adhesive cured (Fig. 2). The adhesive for the first support was allowed to cure for 24 h before the second was attached in the same manner and allowed to cure for 24 h. The above procedure was adopted to minimize distortion from the overconstraint applied by the side supports. Measurements of the retroreflected wavefront at each step of the above process differ by <0.1 wave peak-to-valley. This overconstraint

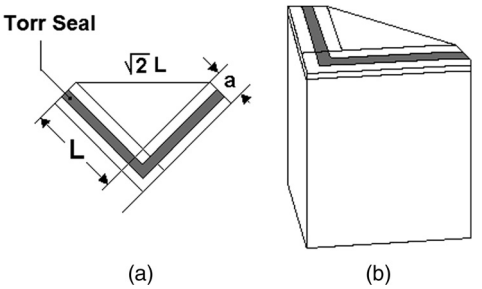

Fig. 2 End brace for the roof mirror. (a) The side supports were attached with a thin (~1 mm) bead of Torr Seal®. (b) After the side support was pressed firmly into place, the assembly was set with the new side support facing up so as to dry under uniform, minimal pressure from its own weight.

distortion is present in the retroreflected wavefront analyzed below and is acceptable for the application demonstrated here.

Finally, the HRM was bonded into a V groove in a ½ in. diameter cylindrical aluminum base with a flat back surface (for attachment to the piezoelectric transducer). The flat back surface of the base was mounted to the jig with double-sided tape so that one face of the base's V groove would remain horizontal while the other remained vertical, see Fig. 3. A thin piece of paper set an air gap between the vertical side of the V groove and the smaller mirror. The largest mirror was pressed into Torr Seal® on the horizontal surface of the V groove so that only gravity applied pressure across the resting surface while it cured. When bonding the HRM to the aluminum base, the vertical air gap was necessary in order to prevent mechanical interference from misaligning the precision of the bond angle as the Torr Seal® cured. Compared to mounting with adhesive on two surfaces of one mirror element,[30] mounting a retroreflector using adhesive on only one rear surface of one mirror element reduces stress;[31] mounting the one rear surface directly to the metal base[30] (rather than using an intermediate glass bonding surface for enhanced thermal stability[31]) reduces total mass and improves mechanical stability. While cutting the aluminum base at the reflective point of symmetry could reduce the mass further, this was not done to minimize torques on the piezoelectric transducer. After the Torr Seal® had cured for 24 h, the HRMs were placed inside the Fizeau interferometer for final analysis.

3 Results

The retroreflected wavefront from one HRM is shown in Fig. 4. Like an ideal plane mirror, an ideal hollow rooftop with a 90 deg mirror joining angle returns a wavefront

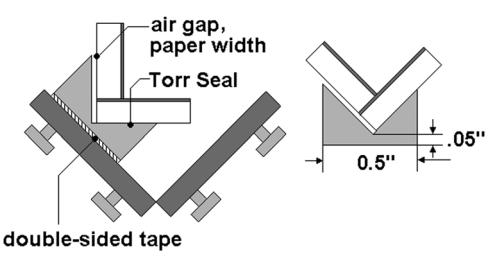

Fig. 3 Mounting the hollow rooftop mirror in the aluminum base. The hollow rooftop mirror was positioned in the base so that gravity exerted uniform pressure on the bond while it dried. Note drawing not to scale.

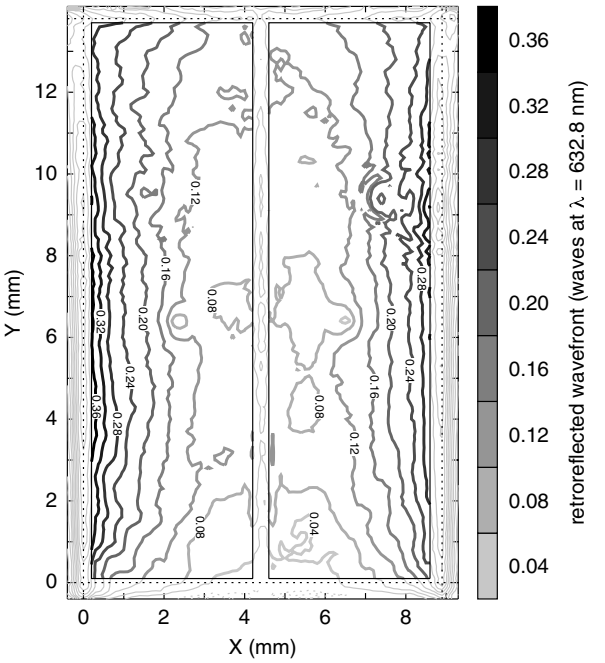

Fig. 4 Contour map of the retroreflected wavefront from the hollow rooftop mirror with 3.2 g mass. The retroreflector clear aperture is enclosed in dashed lines. The usable area is enclosed in two solid rectangles, which exclude the mirror edges and the vertical joint between mirrors and enclose 90% of the clear aperture area (8.9 mm × 13.8 mm). Within the usable area, wavefront contours are indicated in bold grayscale, ranging from 0 to 0.36 waves of the red HeNe (632.8 nm) and labeled as on a topographic map. Outside the usable area, wavefront contours are indicated by uniform light gray contours, with peaks at both vertical edges and a valley in the joint between mirrors. Within the active area, the mean wavefront is at 0.16 waves, the rms wavefront distortion is 0.07 waves, and the peak to valley wavefront distortion is 0.39 waves.

with a flat phase, so the quality of the HRM can be measured with the same surface figures using the Fizeau interferometer. The retroreflected wavefront is symmetrical under reflection across the mirror joint axis (a vertical line at X ~4.4 mm in Fig. 4); asymmetries on the order of 0.04 waves arise from the interferometer. The first standard surface figure is the peak-to-valley wavefront distortion, which measures the maximum retroreflected wavefront difference with respect to a planar surface in units of the 632.8 nm measuring wavelength. The second standard surface figure is the rms wavefront distortion, which measures the root mean square deviation (in waves) of the retroreflected wavefront from a linear fit (the linear fit will remove any retroreflected beam deviation). The first hollow rooftop retroreflector (total mass of 3.4 g for retroreflector and base) had retroreflected wavefront distortions of 0.07 waves rms and 0.38 waves peak-to-valley over 90% of its 8.5 mm × 13.2 mm aperture. Figure 4 shows both the aperture (inside dashed lines) and the 90% usable area (inside boxes chosen to exclude edges and the joint) over which the wavefront distortions are calculated. The second HRM (total mass 3.2 g) had 0.07 waves rms and 0.39 waves peak-to-valley wavefront distortions over 90% of an 8.9 mm × 13.8 mm aperture. The wavefront distortions are slightly less than expected from the mirror specifications. Assuming that symmetrical interferometer distortions have the same magnitude as asymmetrical interferometer

distortions suggests total measurement errors of 0.06 waves peak-to-valley, which is consistent with the agreement between measurements at successive steps in fabrication and with the agreement between the two retroreflectors.

Independent of the angle of incidence within planes perpendicular to the mirror joint axis, a dihedral retroreflector mirror joining angle of $(\pi/2)+\alpha$ will return the incident beam at $\pi+2\alpha$, so that the retroreflector beam deviation is 2α. The maximum ratio of wavefront difference f to lateral distance d determines the worst-case retroreflector beam deviation, $2\alpha=\arctan(f\lambda/d)$. For a simple error in joining angle, the peak-to-valley wavefront difference occurs over a distance of half the clear aperture.[5] With $f_{p-v}=0.38$ wave and using half the clear aperture for the distance, $d_{p-v}=$ 4.2 mm, the retroreflected beam deviation is 5.7×10^{-5} rad (12 s of arc). For the two HRMs, the actual peak-to-valley distance is in one case greater than (and in the other case equal to) half the clear aperture, so these estimates of retroreflected beam deviation are conservative. Over a year after fabrication, the rooftop mirror reflectance measured for p-polarized light at 632 nm wavelength was $95.4\pm0.3\%$, close to that expected in a double pass from the specified 98.3% reflectance of the mirror for unpolarized light.

These low-mass HRMs were used in both arms of a small Mach-Zehnder interferometer mounted on a breadboard on top of a vibration isolated table; the interferometer was open to air. The beams entered the HRMs on one side and left on the other,[6] enclosing an area of ~10 cm^2. A piezoelectric transducer was attached to the back of HRM to actively stabilize the interferometer displacement using feedback from a polarized continuous wave 632.8 nm wavelength HeNe laser.[3,32] Acceleration of the retroreflector during active interferometer stabilization with the piezoelectric transducer is up to $\sim10^{-2}$ g (rms) in a 50 Hz to 3 kHz frequency range. Interferometer displacement was independently monitored outside of the feedback loop using a polarized continuous wave 594.1 nm wavelength HeNe laser.[3] The yellow and red beams were copropagating; the HRMs allowed femtosecond laser beams to be stacked above them inside the interferometer. A displacement stability of ±0.8 nm rms was measured over 0.1 Hz to 10 kHz, demonstrating the structural rigidity of the HRM required for use in actively stabilizing an interferometer.

The retroreflected beam deviation determines the maximum lateral movement of the beam center as the retroreflector is translated. For a 25 mm translation with 12 arc s retroreflected beam deviation, the beam would have a lateral walk off of 1.5 μm. This beam deviation has a minimal effect on use of the interferometer for Fourier transform spectroscopy. By fitting the peak of the Fourier transform (resolution ~0.0005 waves), a scan using steps of one red HeNe wave and a displacement range of 2047 waves measured the number of yellow waves per red wave in air as 1.06543 ± 0.00003. Using a red HeNe wavenumber[33] [in dry air at local atmospheric pressure ($\sim$620 Torr)] of 15,801.6 cm^{-1} leads directly to a yellow HeNe wavenumber of $16{,}835.5\pm0.5$ cm^{-1} in dry air at local atmospheric pressure (yielding 16,831.7 cm^{-1} in vacuum); this compares well to the yellow HeNe wavenumber of 16,832.3 cm^{-1} in vacuum assigned to the energy difference between the Ne $2s^22p^5(^2\mathrm{P}^{\mathrm{o}}_{1/2})5s\ ^2[1/2]^{\mathrm{o}}\ J{=}1$ and $2s^22p^5(^2\mathrm{P}^{\mathrm{o}}_{3/2})3p\ ^2[5/2]\ J=2$ levels.[34,35]

4 Conclusion

Two 3.3 g HRMs with clear apertures of 8.5 mm × 13.2 mm, return beam deviations of 12 arc s, and wavefront distortions of $\sim\lambda/15$ rms at 632 nm were fabricated and tested in actively stabilizing an interferometer. The fabrication technique of directly bonding coated mirrors to each other while measuring and adjusting the dihedral angle might be useful in fabricating other lightweight mirror assemblies. Since the reflective coating of one surface is bonded to the other mirror substrate, the coating can limit the strength of the bond between mirrors. Torr Seal® is useful as a structural adhesive and should allow roof mirrors to be used within a temperature range of −45 to 120°C, but not for the cryogenic applications of Refs. 11 and 14. Compared to the lightest commercially available hollow roof mirrors™ (PLX model RM-10-05, 25 mm × 63 mm clear aperture, 150 g mass, 1 arc s return beam deviation), these HRMs provide 7% of the surface area with 2% of the mass (close to the ratio expected for scaling a cube of uniform density, which does not account for the actual changes in shape, composition, or strength). Typically, rms wavefront distortion increases with retroreflector clear aperture, while the return beam deviation decreases with retroreflector clear aperture; comparisons to trihedral retroreflectors[11,14,17] and hollow penta-prisms[15] are consistent with proportional scaling for both (although fabrication difficulties increase with the number of mirrors). A tongue and groove joint design for the bonded mirror surfaces[11] or alternative cements[11,14,24,25] might lead to improvements. It may also be possible to hollow out the aluminum base to reduce its mass[15] without reducing torsional stability. A merit of the fabrication process is that it does not require a master optical corner cube for reference, but can be constructed using standard optics mounts and a Fizeau interferometer.

The small size of these HRMs allows a smaller and intrinsically more stable interferometer. Assuming the motions required for stabilization are the same, the factor of 50 reduction in mass compared to commercial HRMs reduces the power required to stabilize the interferometer by a factor of 50. Further, a stabilized interferometer's active-feedback bandwidth is often limited by the actuator's mechanical resonant frequencies.[9] Since the resonance frequency is inversely proportional to the square root of the mass, the factor of 50 mass reduction suggests a factor of seven increase in active-feedback bandwidth. Together, these gains have enabled active stabilization of a Mach-Zehnder interferometer so that the displacement was maintained to within ±0.8 nm.

Acknowledgments

This material is based upon hollow rooftop mirror fabrication supported by the Center for Advanced Solar Photophysics, an Energy Frontier Research Center funded by the U.S. Department of Energy, Office of Science, Office of Basic Energy Sciences and interferometric characterization supported by the Colorado Energy Research Collaboratory through the Center for Revolutionary Solar Photoconversion.

References

1. P. Bender et al., "The lunar laser ranging experiment," *Science* **182**(4109), 229–238 (1973).
2. K. Iwasawa, A. Iwama, and K. Mitsui, "Development of a measuring method for several types of programmed tool paths for NC machine

tools using a laser displacement interferometer and a rotary encoder," *Precis. Eng.* **28**(4), 399–408 (2004).
3. M. K. Yetzbacher et al., "Spectral restoration for femtosecond spectral interferometry with attosecond accuracy," *J. Opt. Soc. Am. B* **27**(5), 1104–1117 (2010).
4. S. T. Roberts et al., "A fast-scanning Fourier transform 2D IR interferometer," *Opt. Commun.* **284**(4), 1062–1066 (2011).
5. Z. Bleier, I. Vishnia, and J. Lipkins, "Hollow retroreflectors promote precision optical alignment," *Photonics Spectra* **38**(3), 82–91 (2004).
6. W. H. Steel, *Interferometry*, Cambridge University Press, Cambridge (1967).
7. Y. F. Ma et al., "Greatly improved stability of passively Q-switched Ce: Nd:YAG laser by using corner cube prism," *Laser Phys.* **20**(9), 1802–1805 (2010).
8. C. Dorrer et al., "Spectral resolution and sampling issues in Fourier-transform spectral interferometry," *J. Opt. Soc. Am. B* **17**(10), 1795–1802 (2000).
9. T. C. Briles et al., "Simple piezoelectric-actuated mirror with 180 kHz servo bandwidth," *Opt. Express* **18**(10), 9739–9746 (2010).
10. D. T. Shen, "Frameless hollow roof mirror and method of manufacture," U.S. Patent 7,324,733 B2 (2008).
11. J. J. Lyons and P. A. Hayes, "High-optical-quality cryogenic hollow retroreflectors," *Proc. SPIE* **2540**, 94–100 (1995).
12. H. S. Rana and N. B. Mullett, "Fabrication challenges in large prisms," *Proc. SPIE* **4411**, 140–141 (2002).
13. A. S. De Vany, *Master Optical Techniques*, Wiley, New York (1981).
14. A. Preston and S. Merkowitz, "Hollow retroreflectors for lunar laser ranging at Goddard Space Flight Center," presented at *Int. Technical Laser Workshop 2012*, Session 6: Talk 2, Instituto Nazionale de Fsica Nucleare, Laboratori Nazionali di Frascati, Frascati (Rome), Italy (8 November 2012).
15. P. Yoder, Jr., "High precision 10-cm aperture penta and roof-penta mirror assemblies," *Appl. Opt.* **10**(10), 2231–2234 (1971).
16. M. S. Lipkins, "Method and device for assembling hollow retroreflectors," U.S. Patent 3,936,194 (1976).
17. M. S. Lipkins, "Hollow retroreflector mount," U.S. Patent 3,977,765 (1976).
18. R. J. Hill, Jr., "Enabling two-dimensional Fourier transform electronic spectroscopy on quantum dots," Ph.D. Thesis, Department of Physics, University of Colorado, Boulder (2013).
19. "JML Direct Optics Catalog," Rochester, NY (1993).
20. JML Optical, "Standard reflective coatings," http://www.jmloptical.com/wp-content/uploads/2012/07/Standard-Coatings-Reflective.pdf (19 August 2013).
21. M. Born and E. Wolf, *Principles of Optics*, Pergamon Press, New York (1964).
22. P. F. Forman, "The Zygo interferometer system," *Proc. SPIE* **0192**, 41–48 (1979).
23. C. Ai and J. C. Wyant, "Effect of retroreflection on a Fizeau phase-shifting interferometer," *Appl. Opt.* **32**(19), 3470–3478 (1993).
24. P. R. Yoder, Jr., *Opto-Mechanical Design*, Marcel Dekker, New York (1993).
25. P. R. Yoder, Jr., *Mounting Optics in Optical Instruments*, SPIE, Bellingham, WA (2008).
26. W. E. Bell, "Vacuum sealing of gas laser windows," U.S. Patent 3,390,351 (1968).
27. D. van Vörden et al., "Spring constant of a tuning-fork sensor for dynamic force microscopy," *Beilstein J. Nanotechnol.* **3**, 809–816 (2012).
28. "Technical specifications for Torr Seal (Ladd Research)," http://www.laddresearch.com/torr-sealhttps://www.laddresearch.com/index.php/lanotattachments/download/file/id/182/store/1/ (23 September 2013).
29. A. W. Mix and A. J. Giacomin, "Standardized polymer durometry," *J. Test. Eval.* **39**(4), JTE103205 (2011).
30. Z. Bleier, "Hollow retroreflector assembly with hard mount assembly," U.S. Patent 5,335,111 (1994).
31. J. J. Lyons, III, "Hollow retroreflector assembly with a single bonding surface and single mounting surface mounting member," U.S. Patent 6,902,279 (2005).
32. D. J. Jones et al., "Synchronization of two passively mode-locked, picosecond lasers within 20 fs for coherent anti-Stokes Raman scattering microscopy," *Rev. Sci. Instrum.* **73**(8), 2843–2848 (2002).
33. W.-K. Lee, H. S. Suh, and C.-S. Kang, "Vacuum wavelength calibration of frequency-stabilized He-Ne lasers used in commercial laser interferometers," *Opt. Eng.* **50**(5), 054301 (2011).
34. H. G. Heard and J. Peterson, "Super-radiant yellow and orange laser transitions in pure neon," *Proc. IEEE* **52**(10), 1258 (1964).
35. E. B. Saloman and C. J. Sansonetti, "Wavelengths, energy level classifications, and energy levels for the spectrum of neutral neon," *J. Phys. Chem. Ref. Data* **33**(4), 1113–1158 (2004).

Robert J. Hill is a defect metrology engineer at Intel Corporation. After completing a BS in physics from Purdue University in 2000, he served in the U.S. Air Force, working in a semiconductor laser R&D branch at Kirtland AFB. He recently completed his PhD in physics at the University of Colorado, Boulder, where he worked on enabling optical technology for two-dimensional femtosecond spectroscopy of lead chalcogenide quantum dots.

Trevor L. Courtney earned his BS in chemistry and mathematics from the University of Florida in 2005 and his PhD in chemistry from the University of Colorado in 2012. He is currently a postdoctoral research associate in the Department of Chemistry at the University of Washington, Seattle.

Samuel D. Park earned his BS in chemistry from University of California Berkeley in 2010. He is currently a PhD candidate in chemistry at the University of Colorado, Boulder.

David M. Jonas earned his BS in chemistry and AB in mathematics from University of California Berkeley in 1986, and his PhD in physical chemistry from MIT in 1992. Following postdoctoral work at the University of Chicago, he became a professor in the Department of Chemistry and Biochemistry at the University of Colorado. He is a fellow of the American Physical Society, has served as chair of the International Conference on Ultrafast Phenomena (Optical Society of America), and is a winner of the Ahmed Zewail Award in Ultrafast Science and Technology (American Chemical Society). His research interests include two-dimensional femtosecond spectroscopy and fast electronic dynamics in molecules, photosynthesis, and photovoltaic materials.